International Journal of Environmental Sciences
ISSN: 2229-7359
Vol. 11 No. 20s, 2025
https://theaspd.com/index.php

Performance Analysis Of RIS Machine Learning For Next-Generation Wireless Communication Systems

Akash Mishra[1], Dr. Ritesh Baranwal[2], Prof. Ravi Prakash[3]
[1]M. Tech. Student,ECE , Uma Nath Singh Institute of Engineering and Technology,
Veer Bahadur Singh Purvanchal University, Jaunpur, Uttar Pradesh
[2]Faculty, Department of Electronics Engineering
[3]Faculty,Department of Electronics Engineering

Abstract
By dynamically altering the propagation environment, reconfigurable intelligent surfaces (RIS), which are made up of meta-materials with electromagnetic wave control capabilities, are becoming a key technology in 6G wireless communication. In order to achieve the maximum path gain(dB) at the two receivers provided by only a single transmitter through a couple RIS, this investigation addresses gradient-based optimization of RIS configurations. The phase profiles of the RIS are improved by machine learning approaches, utilizing a training model that employs the Adam optimizer and gradient descent.
This study identifies the RIS area that delivers the greatest path gain improvement through a comparison of the initial path gain to the optimized path gain, with a focusing lens for different RIS areas. The effect of various antenna configurations, such as isotropic, hw_dipole(sionna), dipole and TR 38.901 antennas, on the path gain performance in RIS-assisted communication is also examined in this work. Simulation results illustrate iterative improvements in path gain, indicating the potential of machine learning in setup RIS according to waves with ultimate path gain, fostering 6G and next-generation wireless Communication applications. All simulations are performed using Sionna 0.19.1 and Python 3.9.
Keywords: *Reconfigurable Intelligent surface, Ray-Model, Machine Learning, signal optimization,6G*

INTRODUCTION

The sixth generation (6G) of wireless communication technologies is developing quickly and is predicted to revolutionize connection with previously unknown capabilities [1, 2]. 6G seeks to solve the drawbacks of its predecessors by utilizing state-of-the-art technologies to provide ultra-reliable low-latency communication (URLLC), ultra-high data speeds, and seamless global connectivity [3, 4]. But there are drawbacks to the drive to use ultra-massive MIMO (UM-MIMO) antenna arrays and broaden the spectrum into terahertz (THz) bands, such as considerable path gain loss, signal obstruction and issues with energy efficiency [5-7].
One revolutionary method for improving wireless communication performance is the use of RIS [8, 9]. The wireless propagation environment is dynamically reconfigured by RIS, which is made up of passive components that may change the phase and amplitude of incident electromagnetic waves. By effectively modifying these parameters in light of real-time data, RIS can further optimize its performance when integrated with machine learning [10-11].
Because of its versatility, RIS can improve spectrum efficiency, lower energy costs and lessen signal deterioration in situations when it is in Non-Line-of-Sight (NLoS). RIS has become a key component of 6G research by expanding coverage for high-frequency mmWave and THz bands, so mitigating the inherent constraints of these bands.

LITERATURE REVIEW

The potential of RIS to improve wireless communication has led to a significant advancement. In order to overcome difficulties in RIS-assisted OFDM systems, Qing et al. (2021) [12] suggested an Extreme Learning Machine (ELM)-based channel estimation technique that improves accuracy in spite of hardware flaws. Elshennawy (2022) [13] did away with the necessity for lengthy measurement campaigns by creating a machine learning model for path loss prediction in RIS-assisted systems. Li et al. (2022) [14] investigated how RIS can improve

network performance in a variety of settings and increase 5G coverage. RIS was used to optimize MIMO systems by Perović et al. (2020) [15] in order to improve data speeds and energy efficiency. Zuo et al. (2022) [16] combined RIS with Non-Orthogonal Multiple Access (NOMA) to decrease path loss and boost spectrum efficiency. Hoydis et al. (2024) [17] presented a gradient-based calibration technique for maximizing Channel Impulse Response (CIR) in 6G. In order to optimize RIS reflection coefficients and increase end-to-end data rate in multi-hop networks, Huang et al. (2022) [18] integrated Proximal Policy Optimization (PPO) with Distributed Cascade Backpropagation Network (DCBN).

Even with RIS's tremendous progress, there are still a number of important research gaps. Given the difficulties inherent in dynamic situations, more research into gradient-based optimization techniques is needed to increase path gain accuracy in RIS-assisted systems. While channel prediction has benefited greatly from the successful application of machine learning, its full promise for dynamically modifying RIS phase profiles has not yet met.

By creating a gradient-based optimization methodology to improve the path gain of received signal in RIS-assisted 6G wireless communication systems, this study seeks to address these issues. The phase characteristics of RIS are dynamically adjusted using machine learning approaches to guarantee optimal performance in a variety of settings. This work's main contributions are as follows:

Develop and execute a gradient descent optimization technique: To modify the reflection coefficients of the RIS, aiming to enhance received signal intensity and overall system performance [19-21].

RIS Size and Path Gain Analysis: A thorough examination of the connection between RIS size and path gain that shows how some RIS designs enhance signal transmission.

Path Gain Comparison: To compare the path gain (without optimization) and the optimized path gain via RIS gradient descent optimization, assessing enhancements in the received signal.

Impact of Antenna Types on Path Gain Performance: To compare the path gain (without optimization) and the optimized path gain for each antenna type in order to examine the effects of various antenna configurations, such as isotropic, hw_dipole(sionna), dipole and TR 38.901 antennas,on the path gain performance in RIS-assisted communication.

Python 3.9 is used to run simulations, proving the effectiveness of the suggested strategy.

This paper's remaining sections are arranged as follows: The suggested system architecture and communication situation are explained. After that Signal propagation in the system design is presented. Next the Gradient-Based RIS Optimization framework is explained in more detail. In next Section discusses the findings and analysis. Further concludes with conclusions and suggestions for further research.

System Architecture And Communication Scenario

In order to recreate surroundings, the suggested communication situation is represented inside a wedge geometry [22-24]. The radio material used to make the wedge is composed of metal [25,26], which is an ideal
reflector of electromagnetic waves with a field strength of 1 v/m [27]. The relative permittivity is 1 and the conductivity is 10^7 S/m for the metallic radio
substance [28].

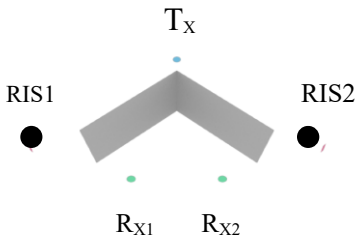

Fig.1: Two RIS Facilitated Transmission with a Wedge and Two Receivers.

In order to highlight the crucial role that RIS plays in signal reradiation, the transmitter and receivers are positioned so that there is no direct line-of-sight (LoS). The two RIS Facilitated Transmission with a wedge and two Receivers is depicted in Figure 1[29,30].

Antenna Transmission

An antenna is used to transmit electromagnetic waves that radiated power requires a comprehension of these fields, which propagate in free space [31-35].

Electric Field of the Electromagnetic Wave:

At a distance r from the antenna, the transmitted wave's electric field is represented as follows:

$$E(r,t) = \left(\frac{E_0}{r}\right)\hat{r}\cos(\omega t - kr) \quad 1$$

Where E_0 is the initial amplitude of the electric field, $\hat{r}$ is the unit vector in the direction of wave propagation, ω is the angular frequency of the wave, k=ω/c is the wave number, in which c is the speed of light, t is the time.

Magnetic Field of the Electromagnetic Wave:

The direction of electromagnetic wave propagation of magnetic field $B(r,t)$ which is perpendicular to both the electric field and the electromagnetic wave propagation direction is given by:

$$B(r,t) = \left(\frac{B_0}{r}\right)\hat{\varphi}\cos(\omega t - kr) \quad 2$$

B_0 is the initial amplitude of the magnetic field, $\hat{\varphi}$ is the unit vector in the direction perpendicular to both the electric field and the EM wave propagation direction.

Transmitted Power from Antenna and Total Radiated Power:

The transmitted power $S(r,t)$ [36] from an antenna:

$$S(r,t) = \left(\frac{1}{\mu_0}\right)E(r,t) \times B(r,t) \quad 3$$

Where μ_0 is the permeability of free space ($\mu_0=4\pi\times10^{-7}$ H/m). The total radiated power P which is represented by:

$$P = \oint S \cdot dA = \left(\frac{1}{2}\right)\eta \int \Omega |E|^2 d\Omega \quad 4$$

Where η is the intrinsic impedance of free space (η=377 Ω), Ω represents the solid angle over which the radiation is distributed.

Analysis Of Signal Propagation In System Architecture

Two carefully positioned Reconfigurable Intelligent Surfaces (RIS1 and RIS2), situated between the antenna and the receivers, receive the broadcast power from the antenna. Depending on the setup and intended signal processing [37], the RISs can modify the broadcast signal by changing their surface characteristics, such as phase profile, amplitude profile [38]. The RIS's reflection coefficients(Γ^1, Γ^2) impact the received power of signal at RIS1 and RIS2. The received power is $P_{RIS1} = \Gamma^1 P$, $P_{RIS2} = \Gamma^2 P$, where P is the total transmitted power from the antenna.

After reflection, the signals go to RX1 and RX2, the receivers, where the received strength is influenced by a number of variables, including distance, propagation circumstances and RIS settings. $P_{RX1} = \alpha^1\Gamma^1 P$, $P_{RX2} = \alpha^2\Gamma^2 P$ can be used to express the received power at each receiver. The path loss factors, α^1 and α^2, take into consideration environmental effects such as fading and shadowing that affect the signal propagation from RIS1 to R_{X1} and RIS2 to R_{X2}, respectively [39].

Thus, $P_{RX1} = \alpha^1\Gamma^1 P$ and $P_{RX2} = \alpha^2\Gamma^2 P$, which takes into account both the reflection coefficients and the path loss factors, provide the total power reaching R_{X1} and R_{X2}.

For R_{X1}, the path gain is:

$$\text{Path Gain}_{RX1}(dB) = 10\log^{10}\frac{(\alpha^1\Gamma^1 P)}{P_{transmitted}} \quad 5$$

Similarly, for R_{X2}, the path gain is:

$$\text{Path Gain}_{RX2}(dB) = 10\log^{10}\frac{(\alpha^2\Gamma^2 P)}{P_{transmitted}} \quad 6$$

Additionally, the Free Space Path Loss (FSPL) is a crucial consideration when assessing signal propagation, the following is the FSPL arithmetic

$$L_{FSPL(r)} = 20 * \log_{10}(r) + 20 * \log_{10}(f) + 20 * \log_{10}\left(\frac{4\pi}{c}\right) \quad 7$$

Where r is the distance between the RIS and the R_X (in meters), f is the frequency (in Hz).

Combining these components allows us to fully comprehend how RISs affect communication systems' signal strength and route loss, providing important information for improving network performance and design in RIS-assisted settings.

RIS Setup and Positioning

The environment is equipped with two RIS units, each of which consists of a collection of passive components that may be configured to alter the amplitude and phase of reflected signals. The RIS's cell count is established via

$$\text{Number of cells} = \left(\text{int}\left(\frac{\text{width}}{0.5\cdot\lambda}\right)\right)^2 \quad 8$$

where λ is the signal's wavelength. The distance between the transmitter (T_X), receiver (R_{X1}, R_{X2}), RIS1, and RIS2 and their corresponding coordinates in X, Y, and Z are mentioned in Table 1.

Table 1: Coordinates and Distance

S.No.		Description	Coordinates	Distance(m)
1		Distance between Tx and R_{x1}	T_X = [-10, 10, 0], R_{X1} = [30, -15, 0]	47.17
2		Distance between Tx and R_{x2}	T_X = [-10, 10, 0], R_{X2} = [15, -30, 0]	47.17
3		Distance between Tx and RIS1	T_X = [-10, 10, 0], RIS1 = [40,10, 0]	50.00
4		Distance between Tx and RIS2	T_X = [-10, 10, 0], RIS2 = [-10, -40, 0]	50.00
5		Distance between RIS1 and R_{x1}	RIS1 = [40, 10, 0], R_{X1} = [30, -15, 0]	26.93
6		Distance between RIS2 and R_{x2}	RIS2 = [-10, -40, 0], R_{X2} = [15, -30, 0]	26.93

Framework For Gradient-Based Ris Optimization

An efficient method for setting up RIS to improve signal strength in wireless communication systems is gradient-based optimization [40,41]. One transmitter, two receivers (R_{X1} and R_{X2}), and two RISs (RIS1 and RIS2) make up the system [42]. The signal y_k that is received at receiver k may be written as follows:

$$y_k = h_k^H \Phi G x + n_k \quad 9$$

Where the channel vector from the RIS to receiver k is represented by $h_k \in C^{M\times 1}$, the RIS phase-shift matrix is represented by $\Phi = \text{diag}\left(e^{j\phi_1}, e^{j\phi_2}, \ldots, e^{j\phi_M}\right)$, the channel matrix from the transmitter to the RIS is represented by $G \in C^{M\times N}$, the transmitted signal is represented by x, and additive white Gaussian noise is indicated by $n_k \sim \mathcal{CN}(0, \sigma^2)$.

For receiver k, the path gain g_k is determined by:

$$g_k = \left|h_k^H \Phi G\right|^2 \quad 10$$

and maximizing the average path gain across all receivers is the optimization goal:

$$\max_{\Phi} \frac{1}{2}\sum_{k=1}^{2} g_k \quad 11$$

Phase shifts $\phi_m \in [0,2\pi]$, amplitude profiles $a_m \in [0,1]$ and mode powers are examples of trainable variables. A gradient-based method is used to adjust these values repeatedly. Using the update rule, the optimization procedure makes use of the Adam optimizer:

$$p_{t+1} = p_t - \eta \cdot \nabla_p \mathcal{L} \quad 12$$

where η is the learning rate and p_t is the parameter at iteration t, $\mathcal{L}$ is the loss function, which is the objective's negative:

$$\mathcal{L} = -\frac{1}{2}\sum_{k=1}^{2} g_k \quad 13$$

The combined CIR for the m^{th} RIS element and k^{th} receiver is:

$$h_{\text{total}} = \sum_{m=1}^{M} \sqrt{\beta_k}\, e^{-j2\pi f_c \tau_{k,m}} \quad 14$$

where f_c is the carrier frequency, $\tau_{k,m}$ is the propagation delay and β_k is the route loss factor.

The Adam optimizer is used to update trainable variables by computing loss gradients until stabilization or a predetermined number of iterations, after initializing them with feasible values [43].

Then, by concentrating energy at certain spots, this optimized RIS, configured as focusing lenses, improves signal strength and performs better than the hand-set RIS profile [44-46].

RESULTS AND DISCUSSIONS

The effectiveness of the suggested gradient-based optimization framework for RIS in enhancing wireless communication is assessed.The simulation parameters are represented in Table 2.

Table 2: Simulation Parameters

Parameter	Value
Carrier Frequency	3 GHz

Parameter	Value
Transmitter Power	44 dBm
RIS Orientation	[0, -PI/2, 0]
RIS Area(m^2)	4, 25, 64, 144, 225
Number of Modes (RIS)	2

The ensuing subsections examine how RIS optimization affects path gain and how RIS configuration, size and proximity affect system performance.

Effect Of Path Gain On Gradient-Based Ris Optimization

The results presented highlight the impact of gradient-based RIS optimization on path gain performance for three cases. (1) Signal received to R_{X1} from transmitter (T_X) without RIS, (2) Signal received by (R_{X1}) via RIS1 and (3) Signal received by R_{X1} via RIS2. Due to the symmetry of the R_X with respect to the RIS and T_X of the system model, the results of the path gain for the second receiver (R_{X2}) are similar to that of R_{X1}. Therefore, in order to keep things brief and prevent duplication, the results for RX2 are not included.

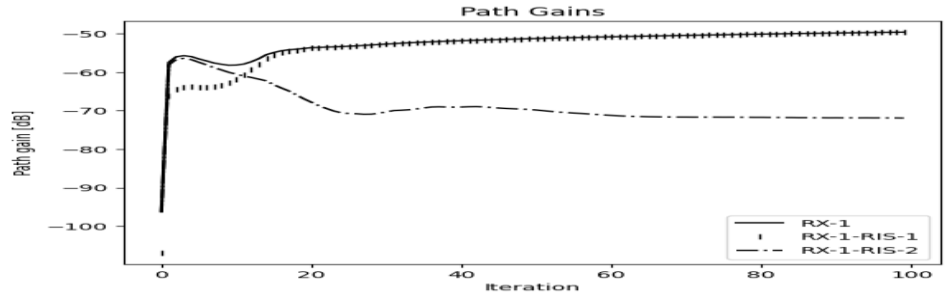

Fig.2: Gradient-Based RIS Optimization Impact on Path Gain(dB) across R_{X1}, R_{X1}-RIS-1, and R_{X1}-RIS-2 Over Iterations

In figure 2 the graph shown by symbol "|" exhibits the greatest improvement in path gain, steeply increasing from -90 dB to stabilize around -50 dB after probably a number of 60 iterations in R_{X1}-RIS-1. This superior performance is attributed to the greater closeness of RIS-1 to R_{X1}.

In contrast, R_{X1}-RIS2 graph is represented by symbol "-." shown an initial improvement, peaks at around -56 dB and then progressively diminishes, stabilizing at -70 dB. The greater distance between R_{X1} and RIS2 as depicted from figure 1 causes more path loss, restricting the improvement in the attainable path. The symbol "-" further highlights the benefit of RIS optimization in which signal received at R_{X1} without RIS is shown. RX1 without RIS stabilizes at about -50 dB, indicating that although the direct connection offers a moderate path gain, its performance is not as good as that of the optimized RIS-1. The performance of RIS-assisted wireless communication systems can be greatly improved by gradient-based optimization in conjunction with careful RIS implementation.

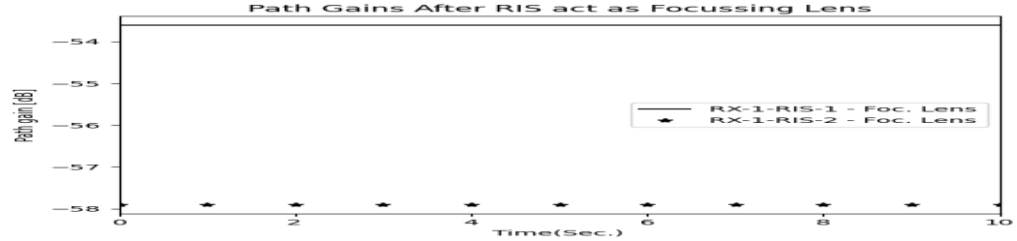

Fig.3: Path Gain(dB) after RIS1, RIS2 act as Focussing Lens

The path gains after learned **RIS1** and learned **RIS2** act as focusing lenses, with an RIS size of 64 m^2 is illustrated in Fig.3. The path gain for **R_{X1} to RIS1** is around **-54.4 dB**, while for **R_{X1} to RIS2** is around **-58.2 dB**. The smaller path gain(dB) for **R_{X1}-RIS2** is due to the longer distance between **R_{X1}** and **RIS2**, compared to the greater closeness of **R_{X1}** to **RIS1**.

RIS Size's Effect on Path Gain

For small RIS area 4 m^2, the path gain before optimization is -98.34 dB, increasing to -77.17 dB after optimization, demonstrating a path gain improvement of -21.17 dB. In a similar vein, RIS areas 25, 64,144 & 225 m^2 exhibit path gain improvements of approximately -36.34 dB, -41.66 dB, -40.33 dB and -37.44 dB respectively, with Optimized path gain with Focussing lens of -60.50 dB, -52.23 dB, -45.31dB & -40.27 dB. The biggest improvement is seen in the 64 m^2 RIS area, in which path gain improvement

by -41.66 dB with optimized path gain of -52.23 dB. Higher initial path gains and Optimized Path Gain with Focusing lens are generally associated with larger RIS sizes. Table 3 looks at how the link between RIS size and path gain (dB) affects both initial and optimized performance.

Table 3: Comparison of Initial, Optimized & Improved Path Gain for different RIS area(m^2).

S.No.	RIS Size (m^2)	Initial Path Gain (dB) with Focussing lens	Optimized Path Gain(dB) with Focusing lens	Path Gain(dB) Improvement
1	2*2	-98.34	-77.17	-21.17
2	5*5	-96.84	-60.50	-36.34
3	8*8	-93.89	-52.23	-41.66
4	12*12	-85.64	-45.31	-40.33
5	15*15	-77.71	-40.27	-37.44

The link between RIS area and initial path gain (dB) as well as the optimized path gain (dB) appears to be plotted in figure 4.

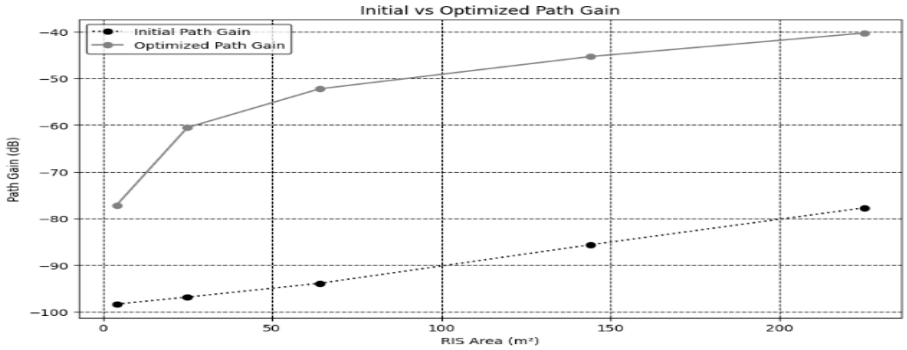

Fig. 4: A comparison of initial path gain, Optimized path Gain for different RIS Area.

The initial path gain often rises in proportion to the RIS area. This implies that improved signal reception may result from a wider RIS region.

Additionally, the optimum path gain rises with the RIS area. Interestingly, the optimized path gain is constantly more than the initial path gain, suggesting that signal reception can be greatly enhanced by adjusting the RIS setup. The improvement in path gain with varying RIS area (m^2) is shown in Figure 5. The improvement in path gain, as indicated by these bars, is -41.66 dB, which is typically higher for RIS areas of 64 m^2 than for RIS area of 4, 25, 144, and 225 m^2, which yield path gains of -21.17 dB, -36.34 dB, -40.33 dB, and -37.44 dB, respectively.

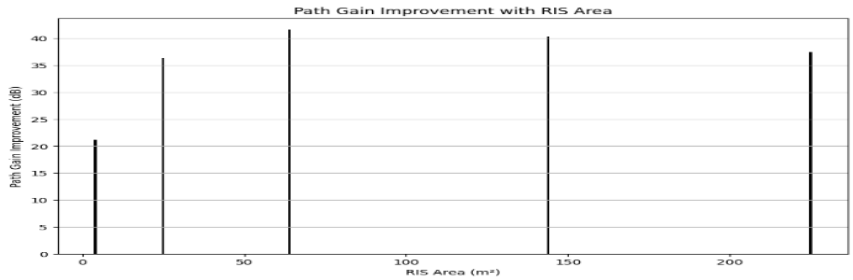

Fig.5: Path Gain improvement with different RIS Area

Additionally, the study shows that, especially under NLoS conditions, 64 m^2 RIS area arrays allow for more efficient compensation for path loss.

The path gain(dB) values for various antenna types are shown in the table 4 both before and after optimization. After optimization, the isotropic antenna's path gain improves to -41.74 dB from its lowest unoptimized value of -77.71 dB. Sionna's hw_dipole performs better at -73.39 dB and then improves to -37.61 dB. Similar improvements are seen with the dipole and TR 38.901 antennas, which have optimal gains of -38.34 dB and -40.48 dB, respectively.

Table 4: Comparison of Path gain with/without optimization for different Antenna at Carrier Frequency of 3 GHz.

S.No.	Antenna Type	Path Gain (without optimization) (dB)	Optimized Path Gain(dB)	Improved Path Gain(dB)
1	Isotropical	-77.71	-41.74	-35.97
2	hw_dipole(Sionna)	-73.39	-37.61	-35.78
3	Dipole	-74.19	-38.34	-35.85
4	TR 38.901	-72.28	-40.48	-31.80

CONCLUSION AND FUTURE WORK

This study shows how effective a gradient-based RIS optimization method is at enhancing wireless communication, especially in NLoS situations.

According to the results, RIS greatly increases path gain and bigger RIS sizes offer better path loss compensation. If the RIS is properly positioned for best performance, the suggested optimization framework's quick convergence makes it ideal for real-time applications.

In order to enable dynamic, real-time responses to changing conditions, future research could concentrate on optimizing path gain through the integration of optimal gradient-based RIS with 5G/6G networks. The hw_dipole (Sionna) shows the greatest boost in path gain, however optimization significantly improves other antenna types. This implies that wireless communication performance can be effectively improved by optimization based on machine learning.

REFERENCES

1. Bourdoux et.al., "6G white paper on localization and sensing," Jun.,2020, arXiv:2006.01779.
2. A. Alkhateeb et al., ''Deep Sense 6G: A large-scale real-world multi-modal sensing and communication dataset,'' 2022, arXiv:2211.09769.
3. J. Hoydis, F. A. Aoudia, A. Valcarce, and H. Viswanathan, "'Toward a 6G AI-native air interface," IEEE Commun. Mag., vol. 59, no. 5, pp. 76–81, May 2021.
4. New SID on AI/ML for NR Air Interface, document RP-212708, 3GPP TSG RAN#94e. 2021.
5. R. Charbonnier et al., "Calibration of ray-tracing with diffuse scattering against 28-GHz directional urban channel measurements," IEEE Trans. Veh. Technol., vol. 69, no. 12, pp. 14264–14276, 2020.
6. Alkhateeb, S. Jiang, and G. Charan, "Real-time digital twins: Vision and research directions for 6G and beyond," 2023, arXiv:2301.11283.
7. X. Lin, L. Kundu, C. Dick, E. Obiodu, and T. Mostak, "6G digital twin networks: From theory to practice," 2022, arXiv:2212.02032.
8. M. D. Renzo et al., "Smart radio environments empowered by reconfigurable AI meta-surfaces: An idea whose time has come," EURASIP J. Wireless Commun. Netw., vol. 2019, no. 1,p. 129, 2019.
9. O. A. Ella, "Performance analysis of the reconfigurable intelligent surfaces communication systems," J. Commun. Inf. Netw., vol. 9, no. 2, pp. 184–191, 2024.
10. R. F. Ibarra-Hernández, F. R. Castillo-Soria, C. A. Gutiérrez, A. García-Barrientos, L. A. Vásquez-Toledo, and J. A. Del-Puerto-Flores, "Machine learning strategies for reconfigurable intelligent surface-assisted communication systems—A review," Future Internet, vol. 16, no. 5, p. 173, 2024.
11. K. M. Faisal and W. Choi, "Machine learning approaches for reconfigurable intelligent surfaces: A survey," IEEE Access, vol. 10, pp. 27343–27367, 2022.
12. C. Qing, L. Wang, L. Dong, and J. Wang, "Enhanced ELM Based Channel Estimation for RIS-Assisted OFDM Systems with Insufficient CP and Imperfect Hardware," arXiv-EESS.SP, 2021.
13. W. S. Elshennawy, "Large Intelligent Surface-Assisted Wireless Communication and Path Loss Prediction Model Based on Electromagnetics and Machine Learning Algorithms," Progress in Electromagnetics Research C, 2022.
14. J. Li et al., "Coverage enhancement of 5G commercial network based on reconfigurable intelligent surface," in 2022 IEEE 96th Vehicular Technology Conference (VTC2022-Fall), 2022.
15. N. S. Perović, L.-N. Tran, M. Di Renzo, and M. F. Flanagan, "Achievable rate optimization for MIMO systems with reconfigurable intelligent surfaces," arXiv [cs.IT], 2020.
16. J. Zuo, Y. Liu, C. Zhu, Y. Zou, D. Zhang, and N. Al-Dhahir, "Exploiting NOMA and RIS in Integrated Sensing and Communication," arXiv [cs.IT], 2022.
17. J. Hoydis et al., "Learning radio environments by differentiable ray tracing," Trans. Mach. Learn. Comm. Netw., vol. 2, pp. 1527–1539, 2024.
18. C. Huang, G. Chen, J. Tang, P. Xiao, and Z. Han, "Machine-learning-empowered passive beamforming and routing design for multi-RIS-assisted multihop networks," IEEE Internet Things J., vol. 9, no. 24, pp. 25673–25684, 2022.
19. M. A. S. Sejan, M. H. Rahman, B.-S. Shin, J.-H. Oh, Y.-H. You, and H.-K. Song, "Machine learning for intelligent-reflecting-surface-based wireless communication towards 6G: A review," Sensors (Basel), vol. 22, no. 14, p. 5405, 2022.
20. J. Hoydis, F. Aït Aoudia, S. Cammerer, M. Nimier-David, and A. Keller. (Dec. 2023). Learning Radio Environments by Differentiable Ray Tracing. [Online]. Available: https://github.com/NVlabs/diff-rt-calibration

21. T. Fugen, J. Maurer, T. Kayser, and W. Wiesbeck, "'Capability of 3-D ray tracing for defining parameter sets for the specification of future mobile communications systems,''IEEE Trans. Antennas Propag, vol. 54, no. 11, pp. 3125–3137, Nov. 2006.
22. T.-M. Li, M. Aittala, F. Durand, and J. Lehtinen, "'Differentiable Monte Carlo ray tracing through edge sampling," ACM Trans. Graph., vol. 37, no. 6, pp. 1–11, Dec. 2018.
23. Recommendation ITU-R P.2040-3: Effects of Building Materials and Structures on Radiowave Propagation Above About 100 MHz, document ITU-R P.2040-3, Aug. 2023.
24. R. G. Kouyoumjian and P. H. Pathak, "A uniform geometrical theory of diffraction for an edge in a perfectly conducting surface," Proc. IEEE, vol. 62, no. 11, pp. 1448–1461, Nov. 1974.
25. Z. Li, "'Neuralangelo: High-fidelity neural surface reconstruction," in Proc. IEEE/CVF Conf. Comput. Vis. Pattern Recognit. (CVPR), 2023, pp. 8456–8465.
26. D. R. Smith, J. B. Pendry, and M. C. Wiltshire, "Metamaterials and negative refractive index," Science, vol. 305, no. 5685, pp. 788–792, 2004.
27. M. Tancik, "'Fourier features let networks learn high frequency functions in low dimensional domains,'' in Proc," Adv. Neural Inf. Process. Syst, vol. 33, pp. 7537–7547, 2020.
28. ITU, "Effects of building materials and structures on radiowave propagation above about 100 MHz," 2015.
29. S. Bakirtzis, J. Chen, K. Qiu, J. Zhang, and I. Wassell, ''EM DeepRay: An expedient, generalizable, and realistic data-driven indoor propagation model,'' IEEE Trans. Antennas Propag., vol. 70, no. 6, pp. 4140–4154, Jun. 2022.
30. Samorzewski and A. Kliks, "Signal Propagation in RIS-Aided 5G Systems," 2024 20th International Conference on Wireless and Mobile Computing, Networking and Communications (WiMob), pp. 443–448, 2024.
31. Balanis, Antenna Theory: Analysis and Design. Hoboken, NJ, USA: Wiley, 1997.
32. Degli-Esposti, V.-M. Kolmonen, E. M. Vitucci, and P. Vainikainen, "'Analysis and modeling on co- and cross-polarized urban radio propagation for dual-polarized MIMO wireless systems,'' IEEE Trans. Antennas Propag, vol. 59, no. 11, pp. 4247–4256, 2011.
33. G. A. Deschamps, "Ray techniques in electromagnetics," Proc. IEEE, vol. 60, no. 9, pp. 1022–1035, Jun. 1972.
34. J. C.-Q. A. L´opez-Aguilar, "Propagation of Electromagnetic waves in material media with Magnetic Monopoles," Progress In Electromagnetics Research, vol. 110, pp. 267–295, 2010.
35. C. Muller, Foundations of the mathematical theory of electromagnetic waves. Berlin, Germany: Springer, 2013.
36. G. Pan, Y. Li, Z. Zhang, and Z. Feng, "Isotropic radiation from a compact planar antenna using two crossed dipoles," IEEE Antennas Wirel. Propag. Lett., vol. 11, pp. 1338–1341, 2012.
37. G. C. Alexandropoulos, G. Lerosey, M. Debbah, and M. Fink, "Reconfigurable Intelligent Surfaces and metamaterials: The potential of wave propagation control for 6G wireless communications," arXiv [eess.SP], 2020.
38. Y. Zhang, J. Zhang, M. D. Renzo, H. Xiao, and B. Ai, "Performance analysis of RIS-aided systems with practical phase shift and amplitude response," IEEE Trans. Veh. Technol., vol. 70, no. 5, pp. 4501–4511, 2021.
39. Choromanska, M. Henaff, M. Mathieu, G. Ben Arous, and Y. LeCun, ''The loss surfaces of multilayer networks,'' in Proc. 18th Int. Conf. Artif. Intell. Statist., San Diego, CA, USA, vol. 38, May 2015, pp. 192–204.
40. Yi, W. Chen, Q. Wu, and H. Wang, ''Machine learning-assisted calibration for ray-tracing channel simulation at centimeter-wave and millimeter-wave bands,'' IEEE Antennas Wireless Propag. Lett., vol. 23, pp. 1623–1627, 2024
41. J. Hoydis et al., ''Sionna RT: Differentiable ray tracing for radio propagation modeling,'' 2023, arXiv:2303.11103.
42. L. Azpilicueta, M. Rawat, K. Rawat, F. M. Ghannouchi, and F. Falcone, "'A ray launching-neural network approach for radio wave propagation analysis in complex indoor environments," IEEE Trans. Antennas Propag, vol. 62, no. 5, pp. 2777–2786, 2014.
43. Gupta, J. Du, D. Chizhik, R. A. Valenzuela, and M. Sellathurai, "'Machine learning-based urban canyon path loss prediction using 28 GHz Manhattan measurements,'' IEEE Trans. Antennas Propag., vol. 70, no. 6, pp. 4096–4111, Jun. 2022.
44. H. Zhou, C. Hu, and X. Liu, "An overview of machine learning-enabled optimization for reconfigurable intelligent surfaces-aided 6G networks: From reinforcement learning to large language models," arXiv [cs.NI], 2024.
45. B. Peng, K.-L. Besser, R. Raghunath, V. Jamali, and E. A. Jorswieck, "RISnet: A Scalable Approach for Reconfigurable Intelligent Surface Optimization with Partial CSI," in GLOBECOM 2023 - 2023 IEEE Global Communications Conference, 2023, pp. 4810–4816.
46. A. C. Pogaku, D.-T. Do, B. M. Lee, and N. D. Nguyen, "UAV-assisted RIS for future wireless communications: A survey on optimization and performance analysis," IEEE Access, vol. 10, pp. 16320–16336, 2022.
47. Z. Yun and M. F. Iskander, "Ray tracing for radio propagation modeling: Principles and applications," IEEE Access, vol. 3, pp. 1089–1100, 2015.
48. S. Bakirtzis, K. Qiu, J. Zhang, and I. Wassell, "'DeepRay: Deep learning meets ray-tracing," in Proc. 16th Eur. Conf. Antennas Propag. (EuCAP), Madrid, Spain, 2022, pp. 1–5.
49. R. Levie, Ç. Yapar, G. Kutyniok, and G. Caire, "'RadioUNet: Fast radio map estimation with convolutional neural networks,'' IEEE Trans. Wireless Commun, vol. 20, no. 6, pp. 4001–4015, 2021.
50. T. Orekondy, K. Pratik, S. Kadambi, H. Ye, J. B. Soriaga, and A. Behboodi, "WiNeRT: Towards neural ray tracing for wireless channel modelling and differentiable simulations," in Proc. Int. Conf. Learn. Represent., 2023, pp.1-19.
51. W. Jakob et al. (2022). Mitsuba 3 Renderer. [Online]. Available: https://mitsuba-renderer.org
52. M. Raissi, P. Perdikaris, and G. E. Karniadakis, "Physics-informed neural networks: A deep learning framework for solving forward and inverse problems involving nonlinear partial differential equations," J. Comput. Phys., vol. 378, pp. 686–707, Feb.2019.
53. B. Nicolet, A. Jacobson, and W. Jakob, "Large steps in inverse rendering of geometry," ACM Trans. Graph., vol. 40, no. 6, pp. 1–13, Dec. 2021.
54. Mildenhall, P. P. Srinivasan, M. Tancik, J. T. Barron, R. Ramamoorthi, and R. Ng, ''NeRF: Representing scenes as neural radiance fields for view synthesis,'' Commun. ACM, vol. 65, no. 1, pp. 99–106, Jan. 2021.